PAPER

Direct ink writing of silica-bonded calcite scaffolds from preceramic polymers and fillers

Biofabrication

PAPER

Direct ink writing of silica-bonded calcite scaffolds from preceramic polymers and fillers

RECEIVED
16 October 2016

REVISED
2 March 2017

ACCEPTED FOR PUBLICATION
10 April 2017

PUBLISHED
11 May 2017

L Fiocco[1], H Elsayed[1,2], D Badocco[3], P Pastore[3], D Bellucci[4], V Cannillo[4], R Detsch[5], A R Boccaccini[5,6] and E Bernardo[1,6]

[1] Dipartimento di Ingegneria Industriale, University of Padova, Via Marzolo 9, I-35131 Padova, Italy
[2] Ceramics Department, National Research Centre, El-Bohous Street, 12622 Cairo, Egypt
[3] Dipartimento di Scienze Chimiche, University of Padova, Via Marzolo 1, I-35131 Padova, Italy
[4] Dipartimento di Ingegneria 'E. Ferrari', Università degli Studi di Modena e Reggio Emilia, Via Vignolese 905, I-41125 Modena, Italy
[5] Institute of Biomaterials, Department of Materials Science and Engineering, University of Erlangen-Nuremberg, D-91058 Erlangen, Germany
[6] Authors to whom any correspondence should be addressed.

E-mail: Aldo.Boccaccini@ww.uni-erlangen.de **and** enrico.bernardo@unipd.it

Keywords: calcite, direct 3D printing, bioactivity, preceramic polymers, biocompatibility

Abstract

Silica-bonded calcite scaffolds have been successfully 3D-printed by direct ink writing, starting from a paste comprising a silicone polymer and calcite powders, calibrated in order to match a $SiO_2/CaCO_3$ weight balance of 35/65. The scaffolds, fabricated with two slightly different geometries, were first cross-linked at 350 °C, then fired at 600 °C, in air. The low temperature adopted for the conversion of the polymer into amorphous silica, by thermo-oxidative decomposition, prevented the decomposition of calcite. The obtained silica-bonded calcite scaffolds featured open porosity of about 56%–64% and compressive strength of about 2.9–5.5 MPa, depending on the geometry. Dissolution studies in SBF and preliminary cell culture tests, with bone marrow stromal cells, confirmed the *in vitro* bioactivity of the scaffolds and their biocompatibility. The seeded cells were found to be alive, well anchored and spread on the samples surface. The new silica–calcite composites are expected to be suitable candidates as tissue-engineering 3D scaffolds for regeneration of cancellous bone defects.

1. Introduction

Calcium carbonate ($CaCO_3$) is a well-established material for implantation purposes, due to its high biocompatibility and bioactivity. As an example, marine corals (99% $CaCO_3$, aragonite polymorph—1% organic) have been used as bone graft substitutes since the 80 s and 90 s [1–4], owing to the distinctive three-dimensional macro-porous framework, naturally mimicking cancellous bone and promoting cell penetration and vascular invasion [4]. From experimental and clinical data, they feature excellent vascularisation, resorbability, biocompatibility and osteoconductivity, so that they can be seen as an interesting alternative to bone grafts [1, 2]. It has been also proven that the bone forming response of calcium carbonate is comparable to that of hydroxyapatite (HAp) [3]; moreover, calcium carbonate is able to induce rapid carbonated apatite formation [4].

Nowadays, implants of natural origin like corals are no longer accepted in orthopedics, due to serious drawbacks, such as supply difficulties, biological variability, risks of viral or bacterial contamination [5]. Therefore, synthetic ceramic biomaterials, chemically and morphologically mimicking natural bone tissue, have received a growing interest in the last years. Several studies have been proposed on synthetic $CaCO_3$ and its polymorphs (calcite, aragonite, vaterite) [5–10]. Monchau *et al* [5] compared the biological properties of synthetic $CaCO_3$ with those of HAp and β-tricalcium phosphate (β-TCP), commonly used as substitutes or filling materials in bone surgery, and demonstrated that synthetic $CaCO_3$ can be shaped into a bone substitute scaffold by slip-casting. The obtained material is non-cytotoxic and facilitates cell proliferation. Similar results were achieved by Lemos and Ferreira [7], who fabricated macroporous $CaCO_3$ by starch consolidation and assessed its accentuated bioactivity. Porous $CaCO_3$ microparticles were also used by Sukhorukov *et al* [10] as a template for encapsulation of bioactive compounds, exploiting the complete biodegradability of $CaCO_3$.

Moreover, Fujita *et al* [9] performed *in vivo* tests in rabbit tibiae to assess the $CaCO_3$ bone bonding ability, showing an adequate bonding strength. So, $CaCO_3$ is an interesting alternative not only to natural coralline aragonite, but also to calcium phosphate ceramics in general.

Further experiences are reported in literature about the synthesis of porous calcite microspheres. For instance, hollow $CaCO_3$ microspheres have been produced starting from water-soluble NaCl cores, covered with $Ca(OH)_2$ by granulation [11]. The external shell was later converted from $Ca(OH)_2$ to $CaCO_3$ by carbonation through a stream of CO_2 saturated with water vapour, whereas the cores were solubilised. Otherwise, hierarchically porous $CaCO_3$ microspheres have been fabricated by a precipitation reaction of $CaCO_3$ in the presence of polystyrene-alt-maleic acid as a crystal modifier, starting from a solution of Na_2CO_3 and $CaCl_2$ [12].

Considering that cancellous bone has a fully interconnected porous structure, a good bone substitute needs a specific morphology, besides a suitable composition. Therefore, porous materials are ideal candidates. Calcite foams have already been fabricated by replica, starting from polyurethane (PU) templates dipped into a slurry of $Ca(OH)_2$ and distilled water [13]. Once infiltrated, the foams have been thermally treated to burn out PU and they have been subsequently exposed to a CO_2 atmosphere to get the carbonation of $Ca(OH)_2$ in $CaCO_3$. Though effective, this method could be simplified using a slurry directly containing calcite, instead of starting with a calcite precursor and then converting it into calcite; anyway, the authors reported to have failed using a calcite slurry, because the foams could not keep their structure after sintering. In fact, it is well known that the thermal decomposition of $CaCO_3$ at high temperature represents a strong limitation to the sintering [14].

In the present study, a technologically advanced method is proposed to fabricate calcite scaffolds with highly ordered open porosity. In particular, we refer to the robocasting of a preceramic paste. This technique relies on direct-writing a continuous ink filament in a layer-by-layer build sequence. Although this technique was developed to print polymers, it nowadays is also possible to generate bioceramic scaffolds [15, 16].

The 3D printable ink was obtained from a solid preceramic polymer (providing SiO_2 in an amount of 35 wt% of the final ceramic) dissolved in isopropanol and mixed with powdered $CaCO_3$ (65 wt%). The polymer-to-ceramic conversion easily allowed the realization of what could be seen as a 'silica-bonded calcite' ceramic composite, in the sense that $CaCO_3$ could be bound by amorphous silica, originated by the thermo-oxidative decomposition of the polymer at a particularly low temperature (600 °C), in agreement with very recent experiments [17]. This strategy differs remarkably from that usually adopted for preceramic polymers and fillers, consisting of treatments above 900 °C, with polymer-derived silica reacting with oxides provided by the fillers ($CaCO_3$, as an example, is a typical source for CaO) [18]. It is also supported by other very recent findings, concerning the biocompatibility of new composite materials deriving from silicones embedding bioglass particles, fired at low temperature [19]. Differently from any previous experiment, the present approach to the synthesis of calcite-containing composites was successfully coupled with direct 3D printing (direct ink writing). Scaffolds showed an abundant open porosity and a remarkable compressive strength, coupled with extremely pronounced biological properties, being able to stimulate the cells proliferation when cultured with bone marrow stromal cells for 2 weeks.

2. Experimental procedure

2.1. Manufacturing of scaffolds

A commercial polymethylsiloxane, SILRES® MK (Wacker-Chemie GmbH, München, Germany), known to have a silica yield of 84 wt% after thermal decomposition in air [20], was used for the fabrication of a 'preceramic ink'. The required amount of silica (35 wt% of the final ceramic) was obtained from two contributions, that is 90 wt% from the silicone resin and 10 wt% from nano-sized silica (fumed silica, Aerosil R106, Evonik Germany). Fumed silica was adopted in order to obtain a silicone-based ink with appropriate rheological behaviour, following previous experiments [21, 22].

Fumed silica powders were wet mixed with MK in isopropanol (8 ml for 16 g of silica precursors) by means of a ball mill (60 min at 100 rpm, Pulverisette 7 planetary planetary ball mill, Fritsch, Idar-Oberstein, Germany). $CaCO_3$ micro-sized powders ($<10\ \mu$m, Industrie Bitossi, Italy) were subsequently incorporated into the polymer and again mixed (4 h at 400 rpm), to obtain a perfectly homogenous suspension with very fine fillers and no trace of powder aggregates. The achievement of such properties was strictly necessary for the direct ink writing, due to the need to avoid clogging throughout the printing step and to have continuity in the fluid flow through the nozzle.

A PowerWASP orienting extruder (Massa Lombarda, Italy), expressly equipped with a syringe to print silicones pastes incorporating fillers, was used to print the preceramic ink (see figure 1(a)). The syringe of the feeding system was filled with the preceramic paste and scaffolds were later printed with conical nozzle (with a diameter of 0.41 mm, Nordson EFD, Westlake, Ohio) immersed in vegetal oil, thus preventing the premature drying of the solvent, that would have affected the viscosity of the ink (see figure 1(b)).

Following the CAD file, scaffolds were in the form of prisms with dimensions 15 mm × 5 mm × 5 mm, as resulting from the overlapping of cylindrical rod, periodically arranged along x and y axes (see figure 1(c)). The rods were in a stacking density of 11

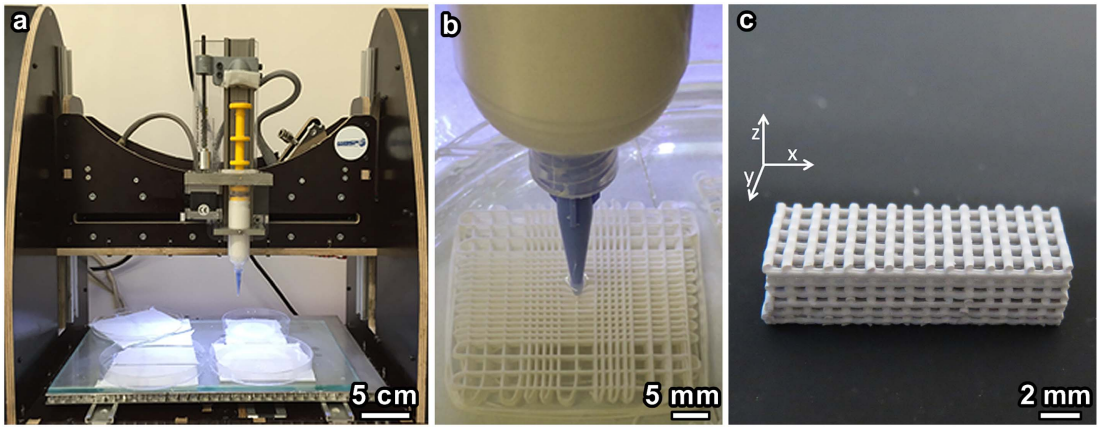

Figure 1. Photographs of (a) the 3D-printer equipped with syringe for silicone-based ink; (b) detail of the printing process carried out in oil bath; (c) overview of a 3D-printed scaffold with orientation of the axes.

rod cm^{-1} on the *x*–*y* plane, and the distance between the longitudinal axes of adjacent rods was of 1 mm. Two different designs were considered for the scaffolds, with a distinction regarding the spacing between adjacent rods along the *z* axis: the spacing was set at 350 μm for samples later referred to as 't-1' design and 300 μm for 't-2' design.

After printing, the scaffolds were left in oil to dry overnight at room temperature. Then, the scaffolds were simply removed from the oil bath and left over paper tissue to take out the excess oil. After removal from the oil, printed scaffolds were cross-linked at 350 °C, with a heating rate of 0.5 °C min^{-1} and dwelling time of 1 h, prior to ceramization at 600 °C in air (same heating rate and dwelling time as the cross-linking treatment), in a chamber furnace (AWF13/12, Lenton, Hope, UK). This relatively low temperature was selected with the aim of getting the thermo-oxidative decomposition of silicone into amorphous silica [17], without affecting the stability of calcite. After 1 h at 600 °C, the ceramized samples were subjected to natural cooling inside the furnace.

2.2. Microstructural and mechanical characterization

Micro-structural characterizations were performed by optical stereomicroscopy (AxioCam ERc 5 s Microscope Camera, Carl Zeiss Microscopy, Thornwood, New York, US), scanning electron microscopy (FEI Quanta 200 ESEM, Eindhoven, The Netherlands) equipped with EDS and x-ray diffraction (XRD; Bruker AXS D8 Advance, Bruker, Germany—CuKα radiation, 0.15418 nm, 40 kV–40 mA, $2\theta = 20°$–$70°$, step size = 0.05°, 2 s counting time). The Match! software package (Crystal Impact GbR, Bonn, Germany) was used for phase identification, supported by data from PDF-2 database (ICDD-International Centre for Diffraction Data, Newtown Square, PA, USA).

The bulk density (ρb) of the foams was determined using a caliper and a digital balance. The skeletal density (ρs) was measured on foams, using a He gas pycnometer (Micromeritics AccuPyc 1330, Norcross, GA), while the true density (ρt) of the material was measured on very finely ground powders of scaffolds. The percentage of porosity (%*P*) was then calculated using the following equation:

$$\%P = 1 - (\rho b/\rho s). \quad (1)$$

Selected scaffold structures were subjected to mechanical characterization in compression mode at room temperature, using an Instron 1121 UTM (Instron Danvers, MA, USA) with a cross-head speed of 1 mm min^{-1}. Each data point is presented as the mean value of five to ten samples.

2.3. Assessment of the in vitro bioactivity

Scaffolds with weight of 100 mg were immersed in 25 ml of simulated body fluid (SBF) solution and stored in an incubator (MPM Instruments s.r.l., Bernareggio, Milano, Italy) at 37 °C. The solution was periodically refreshed (every about 48 h) and the pH of the SBF was measured. After 1, 3, 7 and 14 days the samples were removed from the medium, washed in distilled water and dried at room temperature for 24 h. The potential formation of a hydroxycarbonate apatite (HCA) layer on the samples surface was investigated by means of direct observation in a SEM, operated in low-vacuum mode with a pressure of 0.57 Torr. In addition, a local chemical analysis was performed by X-EDS (Inca; Oxford Instruments, Buckinghamshire, UK). The chemical nature of the precipitated HCA was also investigated by means of micro-Raman spectroscopy (Horiba Jobin-Yvon, Villeneuve d'Ascq, France). A 632.8 nm diode laser with an output power of 20 mW without any filter was employed. The laser was focused on the scaffolds surface by means of 50× and 100× objectives.

Special immersion tests were performed to determine the *in vitro* dissolution of the scaffolds, which were stored in SBF for 2, 4, 8 h; 1 3, 7 and 14 days. At each time point, the pH was measured and samples of 1 ml of the

medium were taken and refreshed. After dilution with 9 ml of 2 M HNO_3, the reacted medium was analysed by inductive coupled plasma (ICP) spectroscopy (ICP-MS, Agilent Technologies 7700 × ICP-MS system, Agilent Technologies International Japan, Ltd, Tokyo, Japan) for Si, Ca, P concentration in solution. The same measurement was performed on the original SBF, which represents a term of comparison. All the experiments were done in triplicate.

2.4. Cell culture test

In this preliminary *in vitro* tests it should be analysed cell attachment and distribution in 3D scaffolds as well as the difference between stimulated and non stimulated cells during a cultivation period of 14 days. Bone marrow stroma contains pluripotential cells with the potential to differentiate into various mesenchymal cell lineages including osteoblasts, adipocytes, chondrocytes and myoblasts [23]. ST-2 cells (from Sigma, Germany), a clonal stromal cell line isolated from bone marrow of BC8 mice, were cultured on the scaffolds. Cells were maintained either in RPMI 1640 containing 10 vol% FBS or for osteogenic stimulation, culture medium was supplemented with 50 mg ml^{-1} ascorbic acid, 10 nM dexametasone and 10 mmol β-glycerophosphate [24].

To observe the formation of the cytoskeleton 'actinring,' the cell distribution and the mineralization process occurring with the scaffolds we used fluorescence microscopy (FM, Scope.A1, Carl Zeiss, Germany). After 14 days of cultivation, adherent cells were fixed with 3.7% paraformaldehyde for 10 min and then permeabilized with 0.1 vol% Triton X-100 (in PBS) for 10 min RT. The fluorescent red-range Alexa Fluor® Phalloidin actin binding compound (Molecular Probes®, Germany) (679 nm excitation and 702 nm emission) was used to detect the cytoskeleton. The fluorescent blue-range DNA binding compound, DAPI (4′,6-diamidino-2-phenylindoledihydrochloride; 350 nm excitation and 465 nm emission) (Roche) was used for detection of nuclei. Briefly, cells were incubated for 60 min with phalloidin (diluted 1:50 by volume) at room temperature followed by an incubation with 1 μg ml^{-1} DAPI for 5 min. Mineralization of the cell culture samples was visualized by sample staining using the OsteoImage™ Mineralization Assay (Lonza, Germany), where the stock solution was diluted 1:100 (v/v) and then subsequently incubated for 30 min at room temperature.

The cell viability of ST-2 cells was measured in a 96 well plate following the conversion of tetrazolium (WST-1, Roche, Germany) to formazan by endogenous enzymes. Culture media was carefully removed completely and fresh media containing 1 v% of the WST-8 Assay Kit solution was added. After an incubation time of 4 h, the absorbance was measured at 450 nm with a microplate reader (PHOmo; Autobio Labtec Instruments Co., Ltd).

After 14 days incubation cell attachment and cell morphology were characterized using scanning electron microscopy (SEM) (Auriga CrossBeam, Carl Zeiss Microscopy GmbH, Germany). Briefly, cell on the scaffold surface were fixed in 3 vol% paraformaldehyde, 3 vol% glutaraldehyde (Sigma-Aldrich, Germany) and 0.2 M sodiumcacodylate (Sigma-Aldrich, Germany). After dehydration through incubation with a series of graded ethanol series (30, 50, 70, 80, 90, 95 and 100 vol%), the samples were critical point dried with CO_2 (EM CPD300, Leica, Germany) and imaged without sputtering.

For statistical analyses, the one-way analyses of variance (Bonferroni's Post hoc test) were used, which are implemented in the Origin software (Origin 8.5 G; OriginLab Corporation) without normality and outlier test. The level of statistical significance was established at $p < 0.05$.

3. Results and discussion

3.1. Morphological and mechanical characterization of scaffolds

The morphological structure of 3D-printed samples was highly regular, as visible in figure 1(c). The open porosity was geometrically ordered and interconnected in all three dimensions (figures 2(a)–(c)). Although the diameter of the nozzle was of 410 μm, the rods were approximately 450 μm in diameter as printed. This was obviously due to the radial expansion of the extrudate occurring when the material leaves the nozzle, caused by the abrupt drop of temperature and pressure. Anyway, after ceramization, the diameter of the rods decreased to approximately 400 μm, due to the shrinkage which usually accompanies the polymer-to-ceramic conversion of preceramic polymers [17].

For t-1 and t-2 designs, the overall morphology was identical, except for the spacing along the z axis (figures 2(b), (c)). As previously mentioned, the spaces between adjacent rods were of 350 μm along the z axis for t-1 design and 300 μm for t-2 design. The reduction of the space along the z axes resulted in a higher mutual interfusion between adjacent layers of rods in t-2 samples, with an increase in the contact area at the joints. Furthermore, in t-2 samples the rods were affected by structural sagging, in comparison to nearly perfect linear rod deposition observed for t-1 samples (figures 2(b), (c)).

The final spacing between adjacent rods on the x–y plane was of approximately 500 μm. This pore size fits well with the requirements for a scaffold for bone tissue engineering. In fact, Hulbert *et al* [25] recommended a minimum pore diameter of 100 μm in their early work, but more recent studies have shown improved osteogenesis for implants with pores greater than 300 μm [26–28].

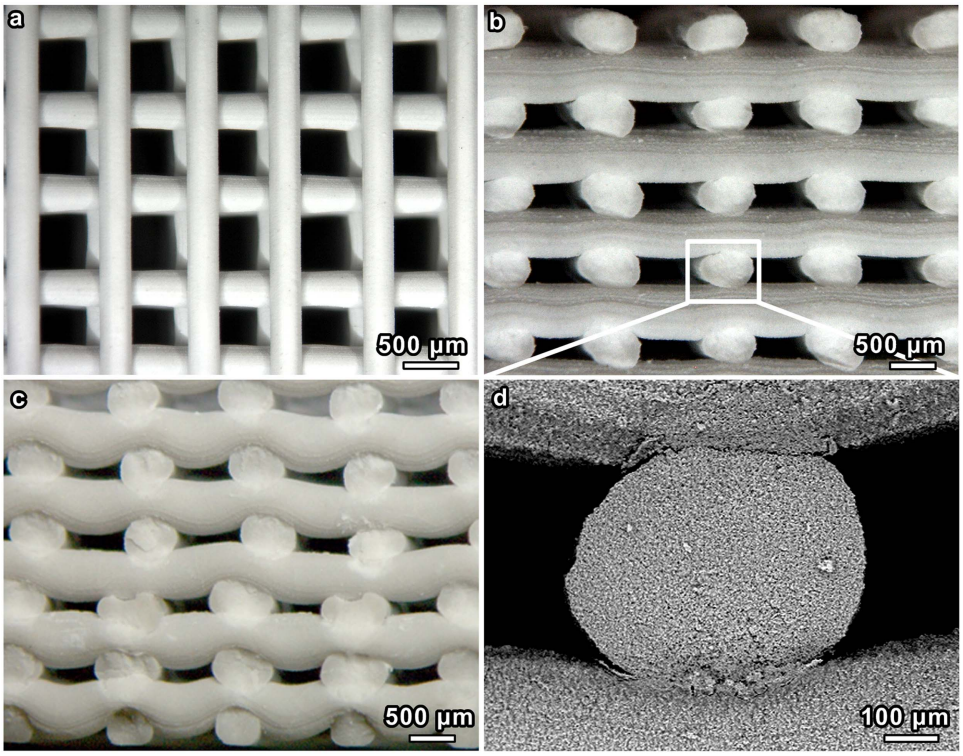

Figure 2. Morphology of 3D printed scaffolds after ceramization: (a) t-1 top view; (b) t-1 side view; (c) t-2 side view; (d) high magnification detail of a rod fracture surface.

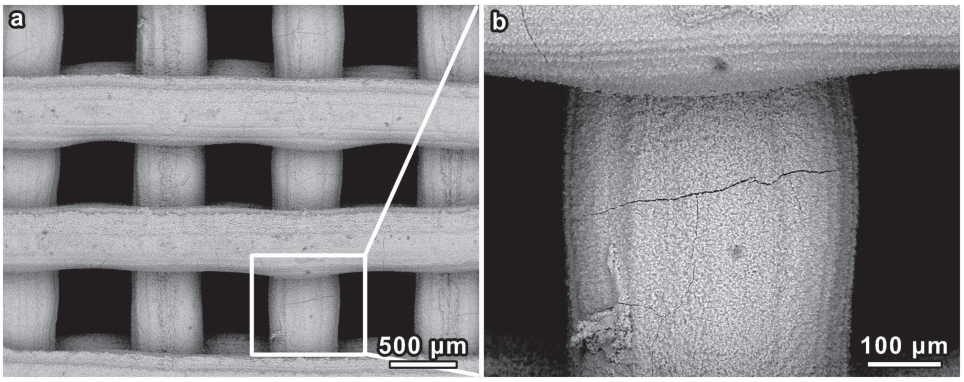

Figure 3. SEM images of t-1 scaffolds after ceramization: (a) top view, (b) higher magnification detail.

Table 1. Summary of physical and mechanical properties of printed scaffolds after ceramization.

Type of geometry	ρ_{bulk} (g cm^{-3})	$\rho_{skeleton}$ (g cm^{-3})	ρ_{true} (g cm^{-3})	P_{open} (%)	σ_{comp} (MPa)
t-1	0.93 ± 0.04	2.56 ± 0.01	2.57 ± 0.01	64	2.9 ± 0.7
t-2	1.07 ± 0.02	2.43 ± 0.04	2.57 ± 0.01	56	5.5 ± 0.3

The higher magnification detail in figure 2(d) reveals that the cross-section of the rods did not contain defects; on the contrary, some microcracks were present on the surface of rods, as shown by figures 3(a), (b), for both designs. The cracks might be reasonably correlated with both the shrinkage of the material and the release of gaseous products throughout the thermo-oxidative decomposition of the silicone, while converting into a ceramic material. Crack generation is typically observed especially in dense polymer-derived-ceramic components, since the elimination of gases can cause local pressure accumulation phenomena [17].

Given the presence of microcracks, the mechanical strength of the developed scaffolds is remarkable: as reported in table 1, the compressive strength (σ_{comp}) was 2.9 ± 0.7 MPa for t-1 samples and 5.5 ± 0.3 MPa

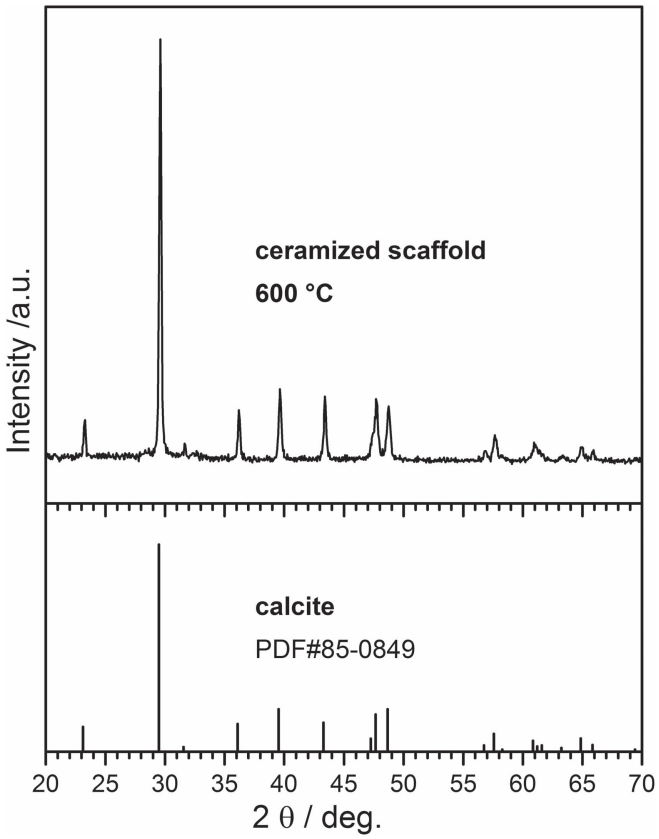

Figure 4. X-ray diffraction patterns of printed scaffolds, after ceramization at 600 °C.

for t-2 ones, respectively. These values are in good agreement with the compressive strength of natural trabecular bone, which is reported to be in the 2–12 MPa range [29]. In particular, for t-2 samples, the standard deviation is quite low, as a proof of high sample reproducibility and more reliable values. The increase in σ_{comp} for t-2 samples compared to t-1 can be explained by several factors. First, it could be correlated with the decrease in open porosity (P_{open}), which was calculated to be 64% for t-1 and 56% for t-2. Then, as already highlighted, rods in t-2 samples had a higher contact area at the joints, due to a higher mutual interfusion between adjacent layers of rods. Finally, the reduced voids in the cross-section could limit buckling phenomena.

A summary of density and porosity values is also presented in table 1. The similarity between skeleton and true density ($\rho_{skeleton}$ and ρ_{true} respectively) is an indicator of limited closed porosity.

The x-ray diffraction patterns presented in figure 4 demonstrate that the thermal treatment at 600 °C of silicone mixed with powdered $CaCO_3$ was effective in maintaining calcite unreacted, while the polymer transformed into silica. In fact, a perfect overlapping between the experimental and the reference pattern of calcite ($CaCO_3$—PDF#85-0849) can be observed, and no other peak appears.

As a final remark on the microstructure, figure 5 demonstrates that both calcium (Ca) and silicon (Si) concentration were practically uniform along the cross-section of rods, so that the calcite filler can be considered to be homogeneously distributed.

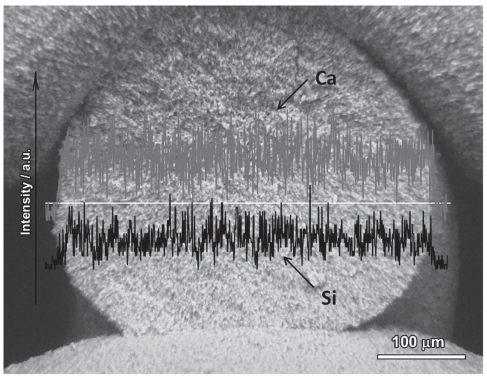

Figure 5. Semi-quantitative SEM-EDS: Ca and Si concentration profiles along the line in a rod cross-section.

3.2. Assessment of the in vitro bioactivity

One of the main features of several bioceramics is the ability to induce the formation of a HCA layer on their surface when exposed to physiological fluids *in vivo*. It is speculated that the growth of this HCA layer is associated with the osseointegration of the implanted material, i.e. its bonding ability to the host bone [30]. It is possible to preliminary assess such property by monitoring the precipitation *in vitro* of a HCA layer on

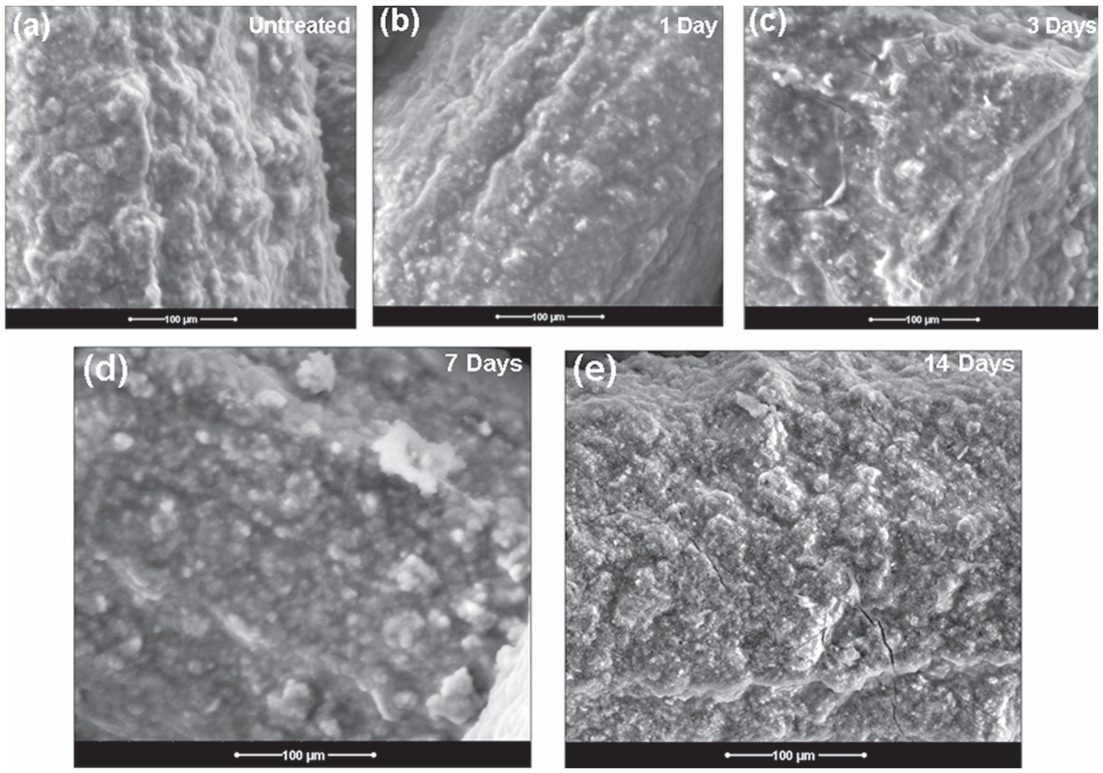

Figure 6. Surface of the scaffolds soaked in SBF for increasing times.

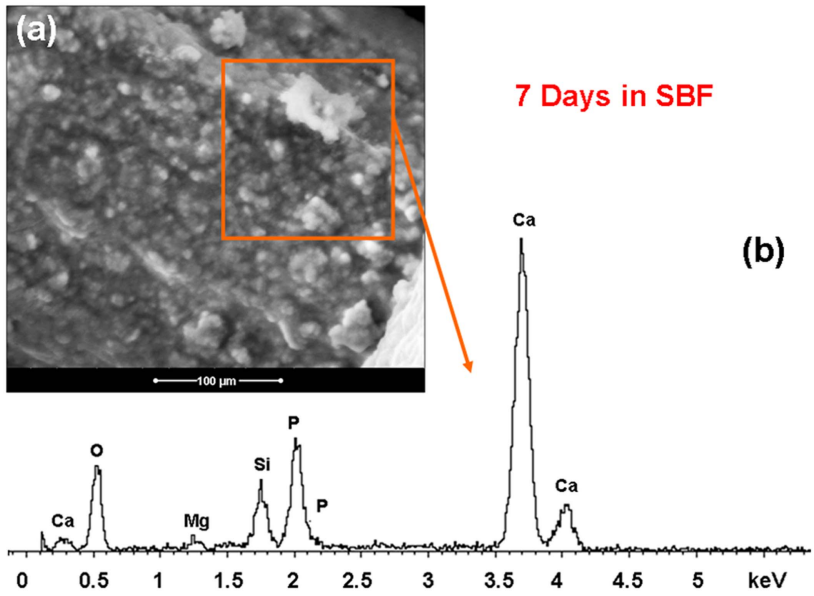

Figure 7. (a) Surface of a scaffold soaked in SBF for 7 days and (b) X-EDS spectrum acquired on the area reported in (a).

the surface of the material, after soaking in SBF for a given period of time. However, such tests should be considered with great caution. In fact, SBF, originally developed by Kokubo and Takadama [31], is just a cellular solution with ion concentrations similar to those of the human plasma (the SBF composition was taken from the literature [31]). As a consequence, it should be stressed that *in vitro* assays are too simple to simulate the real physiological context, which is intrinsically dynamic and includes vitamins, proteins and in particular growth factors, lipids, cells and so forth; so, SBF tests are rather intended to offer a relatively cheap and easy tool to mimic the inorganic reactions which are expected to take place after the implantation of the material. For these reasons, although the apatite formation in SBF is usually considered as an important prerequisite for the subsequent *in vivo* osseointegration, the assessment of

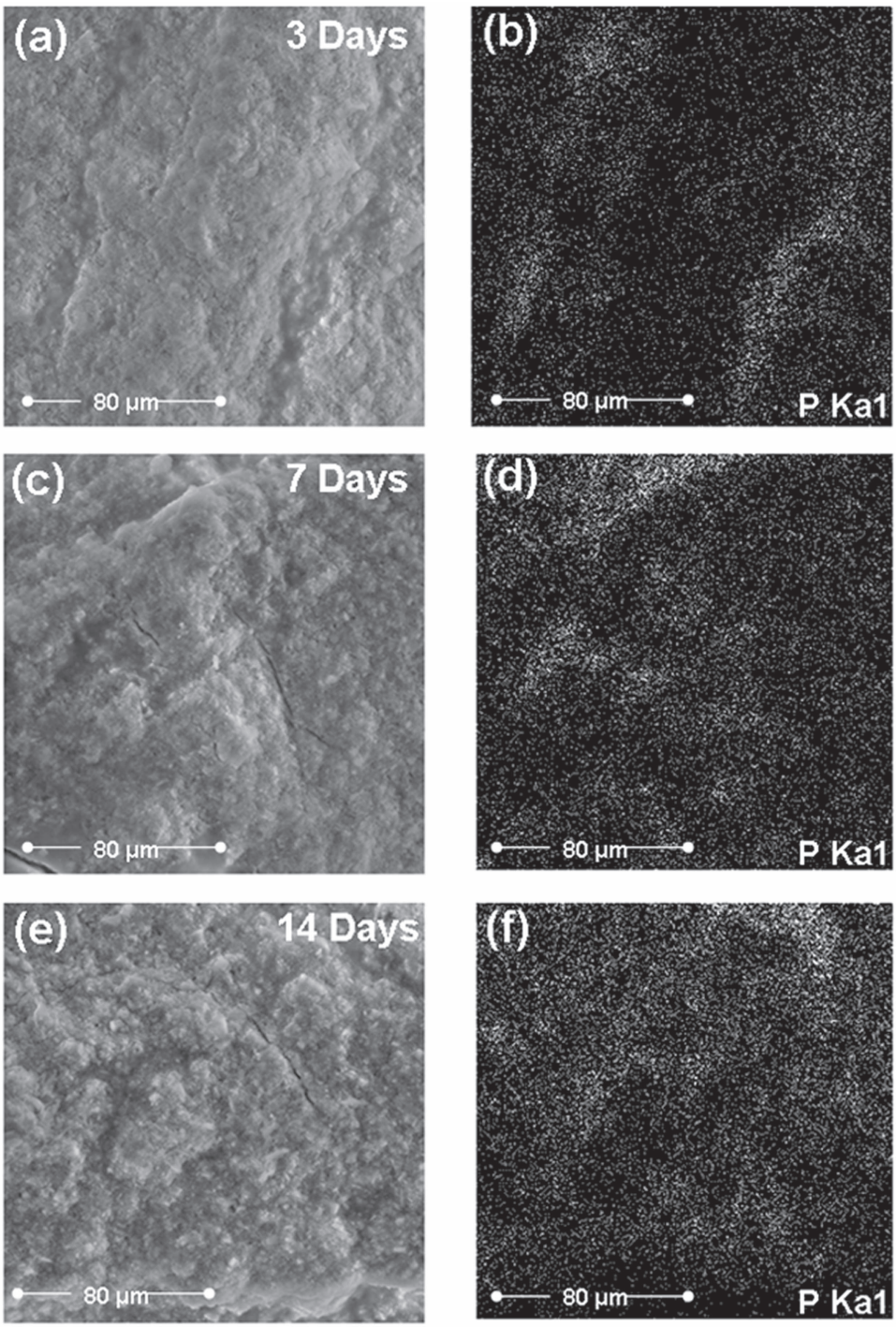

Figure 8. (a), (c), (e) Surface of the scaffolds soaked in SBF for increasing times and (b), (d), (f) X-EDS maps showing the distribution of P, representative of the precipitation of HCA.

the biological responsiveness needs further experimental steps, such as cytotoxicity and genotoxicity assays [32, 33].

The surface of the scaffolds soaked in SBF for increasing immersion times is shown in figure 6. After 7 days in SBF it is possible to locally identify, on the samples surface, several globular precipitates with the typical HCA morphology. The formation of calcium phosphate precipitates on the scaffolds surface after 7 days in SBF is further confirmed by the X-EDS spectra, reported in figure 7, which revealed the presence of phosphorus. On the other hand, a direct SEM observation of the HCA precipitates was instead more difficult for the samples soaked in SBF for 1 and 3 days. However, additional information can be obtained from the X-EDS maps acquired on the samples surface. The X-EDS maps presented in figure 8 show the distribution of P on the samples surface and reveal an increasing amount of P with increasing soaking times. This fact is ascribable to the formation of a thin layer of calcium phosphate precipitates on the scaffolds surface.

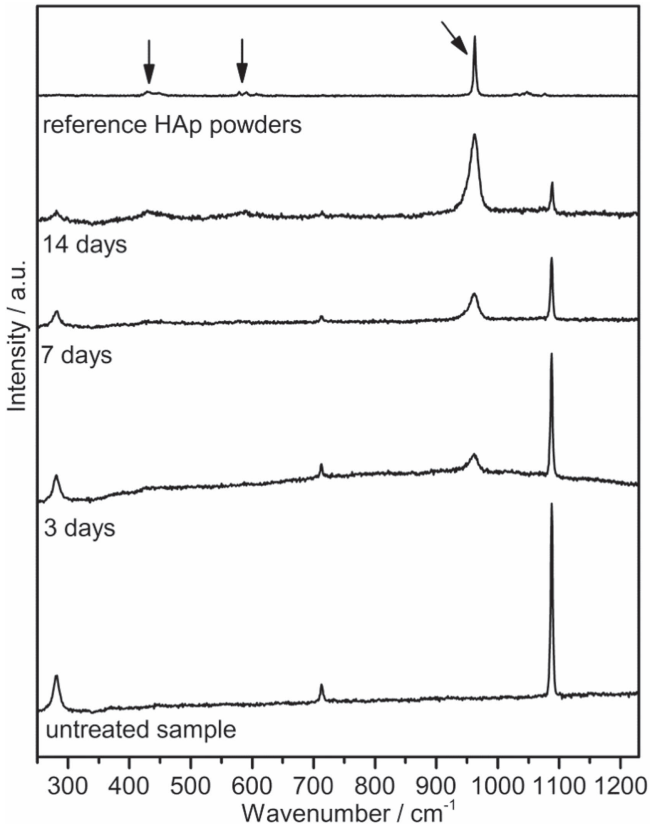

Figure 9. Raman spectra acquired on the samples surface for increasing soaking times, in comparison with the spectrum acquired on an untreated sample (lower pattern) and on HAp powders taken as a reference (upper pattern).

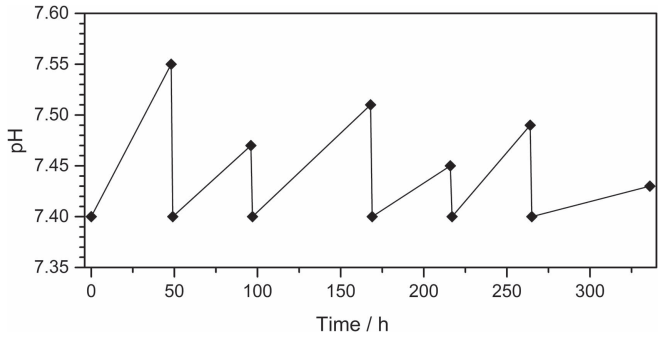

Figure 10. pH variation induced by the samples in SBF; the solution was periodically refreshed.

Within such diffused calcium phosphate matrix, the specific formation of HAC and its increasing amount with time was revealed by means of Raman spectroscopy, which supported the outcomes of the SEM observation. This technique is particularly useful in order to identify the development of HCA, since the Raman peaks related to the vibration of the P–O group are particularly intense and respond as soon as the nucleation of apatite begins. Moreover, it is usually possible to confirm that the *in vitro* grown apatite is carbonated, since the C–O vibrations are also very active in Raman spectroscopy.

The Raman spectra acquired on the samples surface for increasing soaking times are reported in figure 9. The pattern related to the untreated scaffold (lower pattern) shows the typical Raman peaks ascribable to calcite, i.e. an intense sharp Raman band at about 1088 cm^{-1}, which can be assigned to the $\nu_1(CO_3)^{2-}$ symmetric stretching mode, and two bands at about 712 and 282 cm^{-1} [34]. The typical Raman spectrum related to apatite presents a strong peak at about 960 cm^{-1} and two peaks at 590 and 430 cm^{-1}, which are associated to the PO_4 group (see the upper pattern in figure 9). Moreover, a strong peak at about 1070 cm^{-1}, which is related to the stretching of carbonate groups, is ascribable to the specific development of HCA [35–37]. In figure 9 it is possible to observe that the Raman spectra acquired on the samples

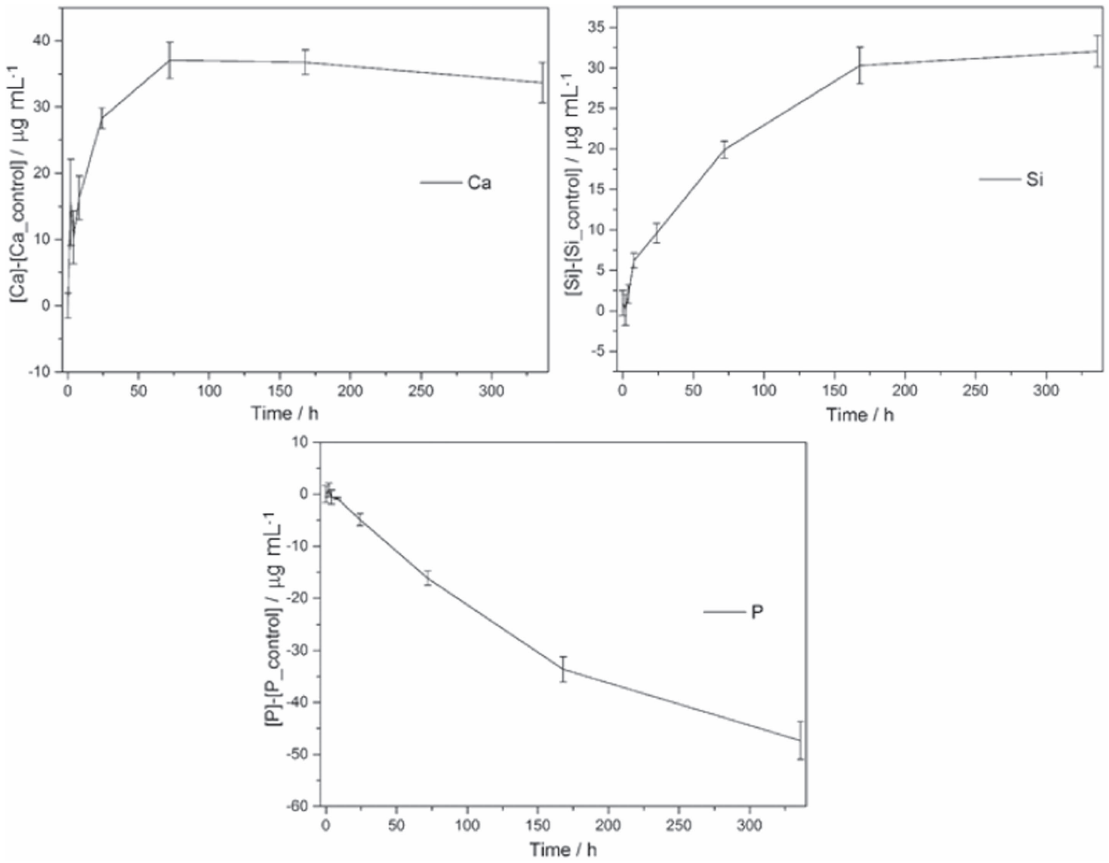

Figure 11. Dissolution profiles as a function of time for the scaffolds after soaking in SBF for 14 days. (a) Ca; (b) Si; (c) P.

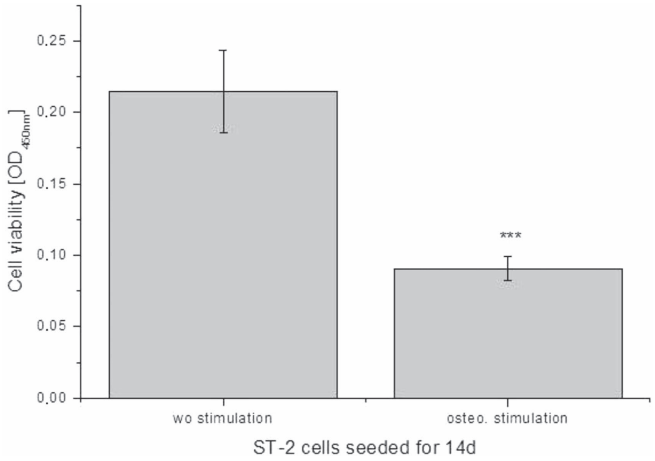

Figure 12. Cell viability of stimulated and non-stimulated bone marrow stromal cells after 14 days of cultivation. (Bonferroni's post-hoc test: $^{***}p < 0.001$).

surface evolve with time and become similar to that of apatite, apart from local fluctuations. However, it should be noted that, for the present samples, the peak at about 1085 cm^{-1}, related to a carbonated group, can be ascribed both to calcite and carbonated apatite.

Particular attention should be paid to the pH variation induced in SBF. In fact, a pH increase is expected when a bioceramic (or a bioactive glass) is immersed in SBF, due to the ion leaching from the sample. On the other hand, cells can be damaged by excessive pH levels (for example, pH values between 7.5 and 8 are usually considered adequate for osteoblasts) or by fast pH variations, and therefore biomaterials characterized by a relatively slow ion leaching should be preferred. If a material is expected to induce dramatic changes of pH, a period of pre-conditioning in SBF can be required to stabilize the pH near to physiological values before further investigations dealing with cells

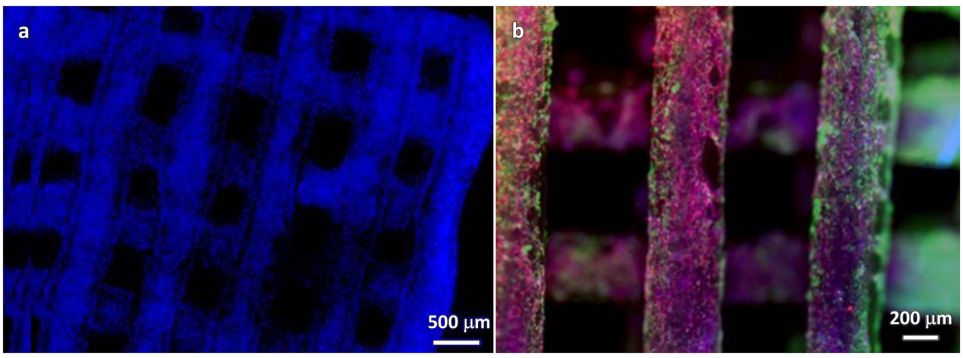

Figure 13. (a) Staining with DAPI shows the cell attachment and distribution after 14 days of cultivation; (b) F-actin (red) staining with rhodamine phalloidin nuclei (blue) staining with DAPI and detection of mineral complexes (green) by OsteoImage throughout the cell culture shows the cell attachment and distribution as well as scaffold mineralisation after 14 days of cultivation.

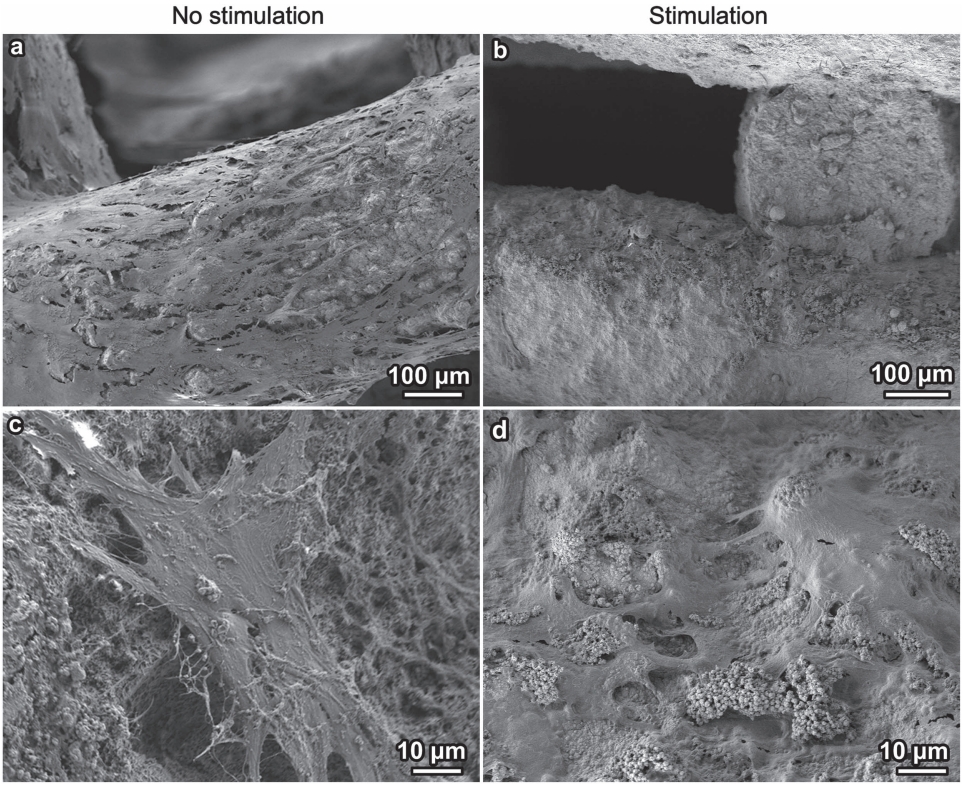

Figure 14. SEM-images of stimulated and non-stimulated ST-2 cells in the scaffolds after 14 days of cultivation.

[38–41]. The pH variation in SBF induced by the produced scaffolds is shown in figure 10. It should be noted that the pH value ranges between 7.4 and 7.6 throughout the process, thus indicating a slow ion leaching. These values are optimal for cell adhesion, proliferation and differentiation. Of course, the pH variation is mitigated by the periodic refresh, but it should be kept in mind that the refreshing procedure is a simplified simulation of the dynamic environment of the human body.

Generally speaking, it is possible to conclude that all the samples showed a relatively slow reactivity *in vitro*, since they were able to develop a calcium phosphate layer with increasing HCA precipitates on their surface during the immersion in SBF.

Figure 11 shows the dissolution profiles for the scaffolds after soaking in SBF for 14 days. These profiles represent the ionic concentrations of Ca, Si and P in SBF, as functions of the contact time, determined by ICP. Ca is contained in SBF and its concentration in SBF containing scaffolds is expected to increase, due to the Ca released by the samples, and then to decrease, due to the reaction with P. On the contrary, Si is not contained in SBF, but it is released by the scaffolds. P is contained in SBF, but is expected to decrease, due to the fact that its presence is involved in the formation of HCA on the samples, by reaction with Ca and subsequent precipitation. A control of pure SBF with no scaffolds immersed was also included in the ICP

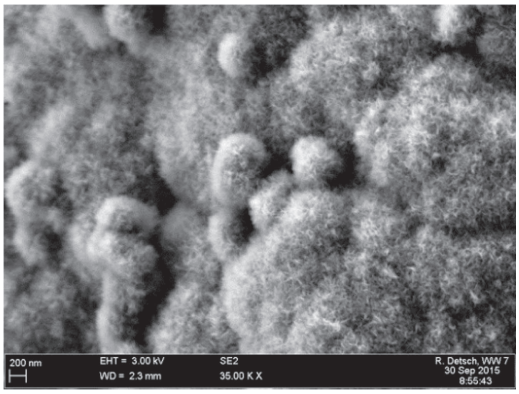

Figure 15. SEM image of the surface after osteogenic cell cultivation.

analysis and its concentrations of Ca, Si and P were subtracted from the analogous concentrations determined in SBF containing the scaffolds. The error bars are standard deviations calculated from triplicates.

The net amount of Si released by the scaffolds reached 30 μg ml^{-1} over 7 days and then was maintained at approximately 30 μg ml^{-1} over 14 days, as shown in figure 11(a).

Following the immersion of the scaffolds, the net content of Ca released by the samples, displayed in figure 11(b), was about 37 μg ml^{-1} over the first 72 h. From 72 h to 14 days, the Ca content began to decrease. Simultaneously, there was a noticeable decrease in concentration of P species in SBF, shown in figure 11(c). Negative values are due to the fact that the concentration of P ions detected in SBF containing the scaffolds was lower than that of pure SBF (as already mentioned, the values represent the subtraction of the concentration determined for pure SBF from that determined for SBF containing the scaffolds). This was likely caused by the deposition, even if weak, of a calcium phosphate layer (HCA) on the surface of the scaffolds after 14 days of immersion, as discussed above.

3.3. Cell culture test

The viability of osteogenic stimulated and non stimulated ST-2 cells on the scaffold surface over the cultivation period was investigated by WST-8 assay. As expected, the viability of ST-2 was significantly higher compared to the osteogenic stimulated cells (figure 12). Therefore, it can be stated that the osteogenic factors supported better cell differentiation than the cell proliferation.

Fluorescence microscope images of scaffolds seeded with non-stimulated ST-2 cells after 14 day are shown in figure 13(a). A homogeneous cell distribution was found throughout all the scaffolds. Cells were comparably attached to the top and bottom surfaces as well as within the pore channels. Similar results were found for ST-2 cell with simulated conditions (data not shown). In figure 13(b) we report one representative image of stimulated ST-2 cells incubated with a scaffold after 14 days of incubation, whereby the cytoskeleton was stained in red, the nucleus in blue and the formed HAp in green. In accordance with figure 13(a), on all samples dense monolayers with cell–cell contacts are visible. Cytoskeleton staining shows clearly smooth and flat formed extensive actin fibres in ST-2 cells on all samples investigated. With help of the green staining, it is possible to visualize HAp formation on the scaffold surface.

SEM images of the top surfaces as well as the inner pore system of scaffolds cultured for 14 days under static conditions are shown in figure 14. These images reveal that the used scaffold material exhibited no cytotoxic effect on the ST-2 cells. Even in the not-stimulated condition ST-2 cells displayed a fibroblastic phyenotype morphology (figures 14(a), (c)). Cell membranes showed blebs and microspikes which indicate high metabolic activities. Stimulated ST-2 cells expressed a typical osteoplastic phenotype on the sample surface (figures 14(b), (d)). All cells on the outer surface of the scaffolds had an osteoblastic cuboidal morphology. The mineral deposit after osteogenic cell cultivation is further shown by figure 15.

4. Conclusions

Silica-bonded calcite has been successfully fabricated by direct 3D printing of silicone/calcite pastes. After cross-linking at low temperature, the printed scaffolds resulted in ceramic components made of calcite surrounded by binding phase of amorphous silica, by ceramization at 600 °C. The decomposition of calcite was prevented by the adoption of a temperature of polymer-to-ceramic conversion far lower than usual for silicone-derived ceramics.

The samples exhibited a highly ordered and interconnected porosity of 56%–64% and a good mechanical behaviour, with a compressive strength of 2.9–5.5 MPa, in good agreement with the requirements of porosity and mechanical strength for scaffold to be used in actual tissue engineering experiments.

Concerning the biological properties, the printed samples were subjected to dissolution study in SBF and cell culture study with bone marrow stromal cells. They showed good *in vitro* bioactivity and very pronounced ability to stimulate cell adhesion and proliferation on the scaffolds surface.

In the light of these encouraging results, the obtained 3D printed silica-bonded calcite composites, from preceramic polymers and fillers, are expected to be suitable candidates for bone tissue engineering applications. Further biological analyses will certainly be performed to assess if the scaffolds can also stimulate cell differentiation and gene expression. In any case, the overall processing, featuring treatments at low temperature, may open the way to a new generation of bioceramics, based on polymer-derived silica embedding bioactive phases.

References

[1] Guillemin G, Patat J L, Fournie J and Chetail M 1987 The use of coral as a bone graft substitute *J. Biomed. Mater. Res.* **21** 557–67

[2] Guillemin G, Meunier A, Dallant P, Christel P, Pouliquen J C and Sedel L 1989 Comparison of coral resorption and bone apposition with two natural corals of different porosities *J. Biomed. Mater. Res.* **23** 765–79

[3] Ohgushi H, Okumura M, Yoshikawa T, Inboue K, Senpuku N, Tamai S and Shors E C 1992 Bone formation process in porous calcium carbonate and hydroxyapatite *J. Biomed. Mater. Res.* **26** 885–95

[4] Ohgushi H 1997 Coral derived porous framework having different chemical compositions as a scaffold for osteoblastic differentitation *Mater. Sci. Forum* **250** 209–20

[5] Monchau F, Hivart P, Genestie B, Chai F, Descamps M and Hildebrand H F 2013 Calcite as a bone substitute. Comparison with hydroxyapatite and tricalcium phosphate with regard to the osteoblastic activity *Mater. Sci. Eng.* C **33** 490–8

[6] Maeda H, Maquet V, Kasuga T, Chen Q Z, Roether J A and Boccaccini A R 2007 Vaterite deposition on biodegradable polymer foam scaffolds for inducing bone-like hydroxycarbonate apatite coatings *J. Mater. Sci., Mater. Med.* **18** 2269–73

[7] Lemos A and Ferreira J M F 2000 Porous bioactive calcium carbonate implants processed by starch consolidation *Mater. Sci. Eng.* C **11** 35–40

[8] Lucas A, Gaudé J, Carel C, Michel J F and Cathelineau G 2001 A synthetic aragonite-based ceramic as a bone graft substitute and substrate for antibiotics *Int. J. Inorg. Mater.* **3** 87–94

[9] Fujita Y, Yamamuro T, Nakamura T, Kotani S, Ohtsuki C and Kokubo T 1991 The bonding behavior of calcite to bone *J. Biomed. Mater. Res.* **25** 991–1003

[10] Sukhorukov G B, Volodkin D V, Günther A M, Petrov A I, Shenoy D B and Möhwald H 2004 Porous calcium carbonate microparticles as templates for encapsulation of bioactive compounds *J. Mater. Chem.* **14** 2073–81

[11] Sunouchi K, Tsuru K, Maruta M, Kawachi G, Matsuya S, Terada Y and Ishikawa K 2012 Fabrication of solid and hollow carbonate apatite microspheres as bone substitutes using calcite microspheres as a precursor *Dental Mater. J.* **31** 549–57

[12] Yu J, Jimmy C Y, Zhang L, Wang X and Wu L 2004 Facile fabrication and characterization of hierarchically porous calcium carbonate microspheres *Chem. Commun.* **21** 2414–5

[13] Maruta M, Matsuya S, Nakamura S and Ishikawa K 2011 Fabrication of low-crystalline carbonate apatite foam bone replacement based on phase transformation of calcite foam *Dental Mater. J.* **30** 14–20

[14] Yamasaki N, Tang W and Ke J 1992 Low-temperature sintering of calcium carbonate by a hydrothermal hot-pressing technique *J. Mater. Sci. Lett.* **11** 934–6

[15] Deisinger U, Hamisch S, Schumacher M, Uhl F, Detsch R and Ziegler G 2008 Fabrication of tailored hydroxyapatite scaffolds: comparison between a direct and an indirect rapid prototyping technique *Key Eng. Mater.* **361–363** 915–8

[16] Gmeiner R, Deisinger U, Schönherr J, Lechner B, Detsch R, Boccaccini A R and Stampfl J 2015 Additive manufacturing of bioactive glasses and silicate bioceramics *J. Ceram. Sci. Technol.* **6** 75–86

[17] Fiocco L, Michielsen B and Bernardo E 2016 Silica-bonded apatite scaffolds from calcite-filled preceramic polymers *J. Eur. Ceram. Soc.* **36** 3211–8

[18] Bernardo E, Fiocco L, Parcianello P, Storti E and Colombo P 2014 Advanced ceramics from preceramic polymers modified at the nano-scale: a review *Materials* **7** 1927–56

[19] Francis A, Detsch R and Boccaccini A R 2016 Fabrication and cytotoxicity assessment of novel polysiloxane/bioactive glass films for biomedical applications *Ceram. Int.* **42** 15442–8

[20] Bernardo E, Colombo P, Dainese E, Lucchetta G and Bariani P F 2012 Novel 3D wollastonite-based scaffolds from preceramic polymers containing micro-and nano-sized reactive particles *Adv. Eng. Mater.* **14** 269–74

[21] Zocca A, Franchin G, Elsayed H, Gioffredi E, Bernardo E and Colombo P 2016 Direct ink writing of a preceramic polymer and fillers to produce hardystonite $Ca_2ZnSi_2O_7$ bioceramic scaffolds *J. Am. Ceram. Soc.* **99** 1960–7

[22] Paquien I-J, Galy J, Gérard J-F and Pouchelon A 2005 Rheological studies of fumed-silica–polydimethylsiloxane suspensions *Colloids Surf.* **260** 165–72

[23] Bianco P, Riminucci M, Gronthos S and Robey P G 2001 Bone marrow stromal stem cells: nature, biology, and potential applications *Stem Cells* **19** 180–92

[24] Schumacher M, Uhl F, Detsch R, Deisinger U and Ziegler G 2010 Static and dynamic cultivation of bone marrow stromal cells on biphasic calcium phosphate scaffolds derived from an indirect rapid prototyping technique *J. Mater. Sci., Mater. Med.* **21** 3039–48

[25] Hulbert S F, Young Y A, Mathews R S, Klawitter J J, Talbert C D and Stelling F H 1970 Potential of ceramic materials as permanently implantable skeletal prostheses *J. Biomed. Mater. Res.* **4** 433–56

[26] Kuboki Y, Jin Q and Takita H 2001 Geometry of carriers controlling phenotypic expression in BMP-induced osteogenesis and chondrogenesis *J. Bone Joint Surg.* **83** S105–15

[27] Tsuruga E, Takita H, Itoh H, Wakisaka Y and Kuboki Y 1997 Pore size of porous hydroxyapatite as the cell-substratum controls BMP-induced osteogenesis *J. Biochem.* **121** 317–24

[28] Götz H E, Müller M, Emmel A, Holzwarth U, Erben R G and Stangl R 2004 Effect of surface finish on the osseointegration of laser-treated titanium alloy implants *Biomaterials* **25** 4057–64

[29] Rahaman M N, Liu X and Huang T S 2009 Bioactive glass scaffolds for the repair of load-bearing bones *Advances in Bioceramics and Porous Ceramics* ed R Narayan and P Colombo vol 32 (New York: Wiley) pp 65–78

[30] Mavrogenis A F, Dimitriou R, Parvizi J and Babis GC 2009 Biology of implant osseointegration *J. Musc. Neur. Interact.* **9** 61–7

[31] Kokubo T and Takadama H 2006 How useful is SBF in predicting in vivo bone bioactivity? *Biomaterials* **27** 2907–15

[32] Bohner M and Lemaitre J 2009 Can bioactivity be tested *in vitro* with SBF solution? *Biomaterials* **30** 2175–9

[33] Gunasekaran S, Anbalagan G and Pandi S 2006 Raman and infrared spectra of carbonates of calcite structure *J. Raman Spectrosc.* **37** 892–9

[34] Sun J, Wu Z, Cheng H, Zhang Z and Frost R L 2014 A Raman spectroscopic comparison of calcite and dolomite *Spectrochim. Acta* A **117** 158–62

[35] Bellucci D, Bolelli G, Cannillo V, Cattini A and Sola A 2011 *In situ* Raman spectroscopy investigation of bioactive glass reactivity: simulated body fluid solution versus TRIS buffered solution *Mater. Charact.* **62** 1021–8

[36] Altomare L *et al* 2011 Microstructure and *in vitro* behaviour of 45S5 bioglass coatings deposited by high velocity suspension flame spraying (HVSFS) *J. Mater. Sci., Mater. Med.* **22** 1303–19

[37] Awonusi A, Morris M D and Tecklenburg M M J 2007 Carbonate assignment and calibration in the Raman spectrum of apatite calc *Tissue Int.* **81** 46–52

[38] Ramp W K, Lens L G and Kaysinger K K 1994 Medium pH modulates matrix, mineral, and energy metabolism in cultured chick bones and osteoblast-like cells *Bone Min.* **24** 59–73

[39] Brandao-Burch A, Utting J C, Orriss I R and Arnett T R 2005 Acidosis inhibits bone formation by osteoblasts *in vitro* by preventing mineralisation calc *Tissue Int.* **77** 167–74

[40] Bellucci D, Cannillo V, Sola A, Chiellini F, Gazzarri M and Migone M 2011 Macroporous bioglass® -derived scaffolds for bone tissue regeneration *Ceram. Int.* **37** 1575–85

[41] Bellucci D, Sola A and Cannillo V 2012 Low temperature sintering of innovative bioactive glasses *J. Am. Ceram. Soc.* **95** 1313–9